Experimental evolution of cellular miniaturization reveals a mechanism for cell size evolution

Garoña A.[1], Lemos V. M.[1], Giometto A.[2], Fumasoni M[1#].

[1] Gulbenkian Institute for Molecular Medicine (GIMM), Oeiras, Portugal

[2] Cornell University, School of Civil and Environmental Engineering, Ithaca, USA

[#] To whom correspondence may be addressed: marco.fumasoni@gimm.pt

ABSTRACT

Cell volume, a key determinant of physiology, is maintained by cell size homeostasis. Large deviations from typical size are often harmful, yet cell sizes have diverged drastically in evolution. How does size homeostasis evolve to support such diversity without impairing physiology? To address this, we used experimental evolution to select progressively smaller *Saccharomyces cerevisiae* cells. Over 1,500 generations, we achieved a six-fold volume reduction compared to wild type. Size homeostasis remained robust and evolutionary stable, with cells maintaining competitive fitness, indicating that dramatic volume changes need not compromise physiology. We investigated the genetic basis of cellular miniaturization through whole-genome sequencing of the evolving populations. We show that genetic manipulations of the G1 cyclin *CLN3* and the Greatwall kinase *RIM15* signaling cascades produce a fourteen-fold change in cell size, with adaptive mutations recapitulating the evolved volumes and loss-of-function mutations yielding enlarged cells. Our results demonstrate the evolutionary plasticity of cell size homeostasis and reveal a mechanism for eukaryotic cell size evolution.

Significance statement

Cell size affects nearly every aspect of cell function and varies enormously among eukaryotes. How such diversity arises while cells remain stable and healthy is not well understood. Using experimental evolution in budding yeast, we selected for progressively smaller cells and identified mutations in conserved cellular pathways that enable stable size reduction without major fitness costs. These results show that gradual evolutionary tuning of core regulatory networks can support large changes in cell size while preserving normal function, providing an experimental framework to explore how fundamental cellular traits evolve.

INTRODUCTION

Cells are the fundamental unit of life, and their size is a key determinant of cell and organismal physiology (1). Through its effects on biosynthesis and proliferation, cell size constrains tissue architecture and regulates functional specialization (2–4).

Not surprisingly, cell size varies greatly across the tree of life. Among prokaryotes, cell diameters range from ~0.2 μm in *Mycoplasma* species (5) to nearly 1 cm in *Thiomargarita magnifica* (6). Eukaryotes exhibit a similarly broad distribution, from the smallest known free-living species *Ostreococcus tauri,* with a 1–2 μm diameter (7), to 15 cm long ostrich eggs (8). Even within multicellular organisms, as in humans, cells range from lymphocytes (<10 μm) to meter-long neurons (9).

Despite this large variability, specific cell types typically maintain their size within a narrow range through a process defined as cell size homeostasis (10, 11). At its core, cell size homeostasis relies on the precise coordination of cell growth and division. The most direct evidence of such control on cell size is that cells born small typically grow more before dividing, and vice versa (12). While, in theory, size control could be performed throughout the

48 cell cycle (13), most organisms exert it mainly prior to DNA synthesis, such as in budding yeast
49 (14) and humans (15), or before nuclear division, such as in fission yeast (16). The general
50 principles followed by cells to regulate their size, as well as the molecular mechanisms that
51 execute this control, have been studied and debated for decades. These are best understood
52 in the budding yeast *S. cerevisiae*, where cells are thought to commit to division once they
53 reach a critical size (14) or after adding a constant volume each cycle (17). The mechanism
54 that determines the transition from G1 to S phase has been proposed to depend mainly on
55 titration of cell cycle activators (e.g. Cln3), inhibitors (e.g. Whi5), transcription factors (e.g.
56 SBF), or their combination (for detailed mechanisms, see refs. (18–25)).

57 Strong evidence for the importance of cell size homeostasis is represented by the severe
58 defects experienced by cells as they leave their narrow range of stereotypical sizes. Excessive
59 cell growth has been shown to cause cytoplasm dilution and genetic instability, ultimately
60 increasing cells' propensity to senescence (26–33). On the other hand, mutations causing the
61 largest decrease in cell size impair the Target of Rapamycin (TOR) signaling and ribosome
62 biogenesis, imposing severe reductions in cellular biosynthesis and fitness (34–37). Notably,
63 altered cell size control has been observed in cancers (38–41).

64 It is therefore unclear how evolution has achieved changes in cell size of many orders of
65 magnitude, when even slight increases or decreases are associated with severe cellular
66 defects. These detrimental consequences could severely constrain the evolution of the cell
67 size trait, posing an apparent paradox between the broad evolutionary diversity of cell sizes
68 and the limited tolerance observed within species. To address this paradox, we sought to
69 observe in real time the evolution of a large decrease in cell size in the model eukaryote *S.*
70 *cerevisiae*. To this goal, we resorted to an experimental evolution regime (42–44),
71 simultaneously imposing direct selection of cellular size by Fluorescent-Activated Cell
72 Sorting (FACS), followed by selection for competitive fitness. Applying this regime over 1,500

generations produced miniaturized cells with six-fold reduction over wild type (WT) volumes and bearing only marginal fitness tradeoffs. Miniaturized cells maintained their phenotype in the absence of selection and had tight control over size distribution at the population level. Whole-genome sequencing revealed adaptive mutations in the *CLN3*, *SCH9,* and *RIM15* genes. Collectively, these mutations decouple the tight link between growth rate and cell size by altering the G1 cyclin and Greatwall signaling pathway. Targeted engineering of these pathways rewired cell size control and cell cycle dynamics, yielding a ten-fold range in cell volume. Our work demonstrates the plasticity of the mechanisms governing cell size homeostasis and suggests an effective mechanism for cell size evolution.

RESULTS

To investigate how cell size can evolve under sustained proliferative capacity, we developed an experimental system in *S. cerevisiae* alternating two selective regimes targeting cell size and reproductive fitness, respectively. Cell populations were analyzed by Fluorescence Activated Cell Sorting (FACS), using the light scattered by cells (forward scatter area, FSC-A), a widely used proxy for their size (45). Only the smaller 7% of cells were collected into separate tubes and subjected to a second selection step (Figure 1A, see Materials and Methods and Figure S1A for details). The second selection consisted of the unconstrained growth of the sorted population for at least 11 generations, during which cells competed for resources (Figure 1A). Three parallel small (S1-3) populations were subjected daily to the two selection regimes, for a total of 1,500 generations (Figure 1B). Under these conditions, selection favors mutations that reduce cell size without compromising proliferation. To speed the evolution, the starting haploid population (ancestor) carried a mutator allele in the catalytic subunit of DNA polymerase delta (*pol3-L523D*, (46) Table S1). In addition, we engineered the ancestor strain to express a cytoplasmic fluorescent protein (ymCitrine) to prevent subcellular debris from being sorted.

Over 1,500 generations, the evolving populations (S1–3) showed a gradual decrease in FCS values as measured by flow cytometry (Figure S1B). Microscopy and Coulter counter analyses confirmed that this reduction was accompanied by a marked decrease in cell volume (Figure 1C–D). Literature values from Coulter counter measurements are often reported from log-phase cultures, where the prevalence of daughter cells skews the volume distribution toward smaller sizes. To avoid biases from growth phase and cell cycle differences, we measured volumes at saturation (48 h), which normalizes these effects and yields consistently higher values (Figure S1C). Relative to WT cells (101 fL ± 17 (mean ± SD)), S-populations at 1,500 generations displayed on average a six-fold decrease, reaching 14 fL ± 1.5 (mean ± SD, Figure 1C), a volume closer to the bacterium *B. subtilis* than their own ancestor. Comparatively, perturbations of the TOR signaling pathway (*sch9*Δ and *sfp1*Δ), which produced the smallest previously known yeast cells (34, 47), only reduced volumes by threefold (30 fL ± 1.7 and 28 fL ± 2.8, respectively (mean ± SD)) (Figure 1C). Our selection experiment therefore produced the smallest *S. cerevisiae* cells reported to date, representing, to our knowledge, the largest reduction in cell volume observed in proliferating cells, excluding cases associated with developmental programs and ploidy changes. Comparable reductions in *S. pombe* have been reported to cause mitotic catastrophe (48, 49). Strikingly, the evolved cells reached volumes similar to those of the smallest species within the *Saccharomycotina* subphylum (Figure S1D), spanning nearly half of the natural size diversity observed across the phylum despite over 400 million years of divergence (50).

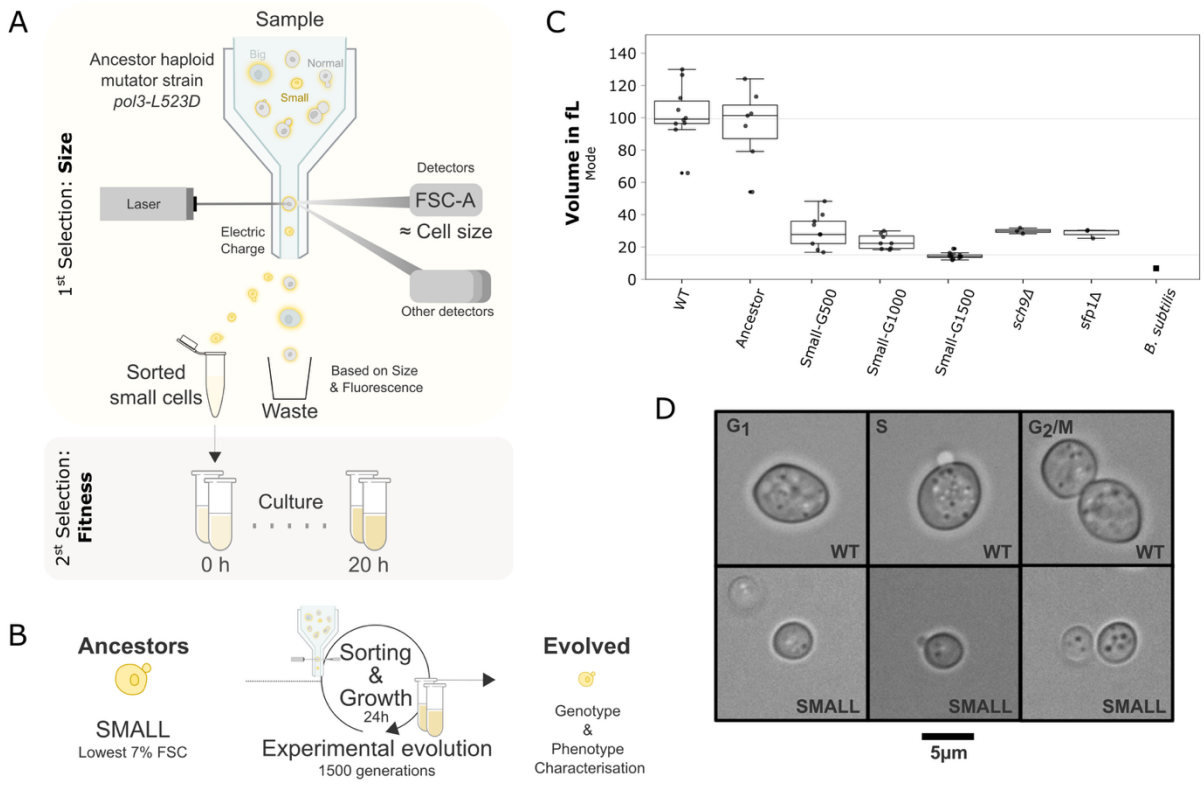

Figure 1. Experimental evolution of cellular miniaturization. (A and B) Schematic representation of size selection and evolution regimes. A haploid *pol3-L523D* mutator ancestor population was sorted into three small (S) subpopulations and subjected to daily size selection. Cells in the lowest 7% of the forward-scatter distribution were sorted (100,000 cells) and cultured in 10 mL rich medium (YPD). Populations were serially grown and sorted for 116 cycles (~1,500 generations), with samples collected and stored every 24 h. (C) Cell volume measurements (Coulter counter) across generations. Data from the three S-populations are plotted together, showing progressive evolution toward smaller size, reaching up to a sixfold reduction in volume. Grey lines indicate wild-type and final evolved sizes. Box plots show medians, interquartile ranges, whiskers (1.5× IQR), and outliers. (D) Light micrographs of wild-type and evolved small-cell populations at different cell-cycle stages (G1, S, G2/M). Scale bar, 5 µm.

Gradual cell size decrease leads to altered morphology and cell cycle dynamics, with marginal fitness tradeoffs.

The dramatic changes in cell volumes observed during our evolution prompted us to examine potential alterations in cellular architecture. First, we focused on intracellular organization, reasoning that reduced volume might occur at the expense of specific organelles. To obtain a general view of subcellular structures, we performed transmission electron microscopy (51) on exponentially growing WT, ancestral, and evolved S-populations. Buds smaller than

136 mother cells, consistent with asymmetric cell division (14), were commonly observed.
137 Interestingly, major organelles displayed their typical morphology, though with altered
138 proportions, suggesting a potential differential miniaturization of organelles (Figure 2A and
139 Figure S2A). Despite the presence of petite mutants (cells lacking functional mitochondrial
140 respiration), most evolved isolates, including the smallest, retained growth on non-
141 fermentable carbon sources, indicating preserved mitochondrial function (Figure S2B).

142 Cell cycle is a major determinant of cell morphology in budding yeast (52). To determine
143 whether changes in cell size were associated with alterations in the cell cycle, we analyzed
144 DNA content in exponentially growing populations, where signal intensity distinguishes cell
145 cycle phases (1C for G1, 2C for G2/M, and 1C < DNA < 2C for S phase). Strikingly, by generation
146 1,500, evolved small cells displayed a near absence of G1 compared with WT (Figure 2B and
147 S2C). Notably, cell cycle changes during evolution occurred in two steps: during the first ~150
148 generations, the proportion of cells in G1 increased, followed by a sharp shift around
149 generation 700 that resulted in the near disappearance of G1 (Figure 2C and S2D). Calculating
150 the absolute time spent in each phase confirmed this trend, showing that the reduction of G1
151 duration was primarily compensated by a corresponding extension of G2/M (Figure 2C-D and
152 S2D).

153 We next examined how changes in cell size and cycle affected population growth. Growth
154 curves of WT, ancestral, and S-populations revealed a marked increase in maximum
155 population density of the evolved lines (Figure 2E). Their growth rates were only marginally
156 reduced relative to ancestors, which themselves grew slower than WT, potentially due to the
157 mutator phenotype (Figure 2F). To precisely estimate this defect, we resorted to pairwise
158 competition assays, which measure relative fitness, a measure of the reproductive success
159 of organisms (53). All three evolved S-populations had equivalent relative fitness ($\omega = -7{,}79\%$
160 $\pm$ 1.4, mean ± SD vs. ancestor), whereas WT showed a ~5% advantage relative to the ancestor

(Figure 2G). In contrast, deletion of *SCH9*, which produces the smallest cells previously reported, caused a severe fitness defect (–28.76% ± 1.1, mean ± SD) despite reducing cell volume only threefold. Across all populations, fitness followed a non-uniform trajectory: (i) declining during the first 200 generations, (ii) recovering by ~250, (iii) dropping sharply until ~500, and (iv) stabilizing with minor decreases until 1,500 (Figure 2H, S2E). Fitness was more strongly associated with cell-cycle dynamics than with cell volume (Pearson $r = 0.67$, $p < 0.001$ for G1 fraction; $r = 0.30$, $p = 0.11$ for cell volume), indicating that changes in fitness primarily reflect alterations in cell-cycle progression (Figure 2I, S2F).

Thus, cellular miniaturization was accompanied by significant changes in cell cycle dynamics while maintaining a substantially higher fitness than previously known small-size mutants.

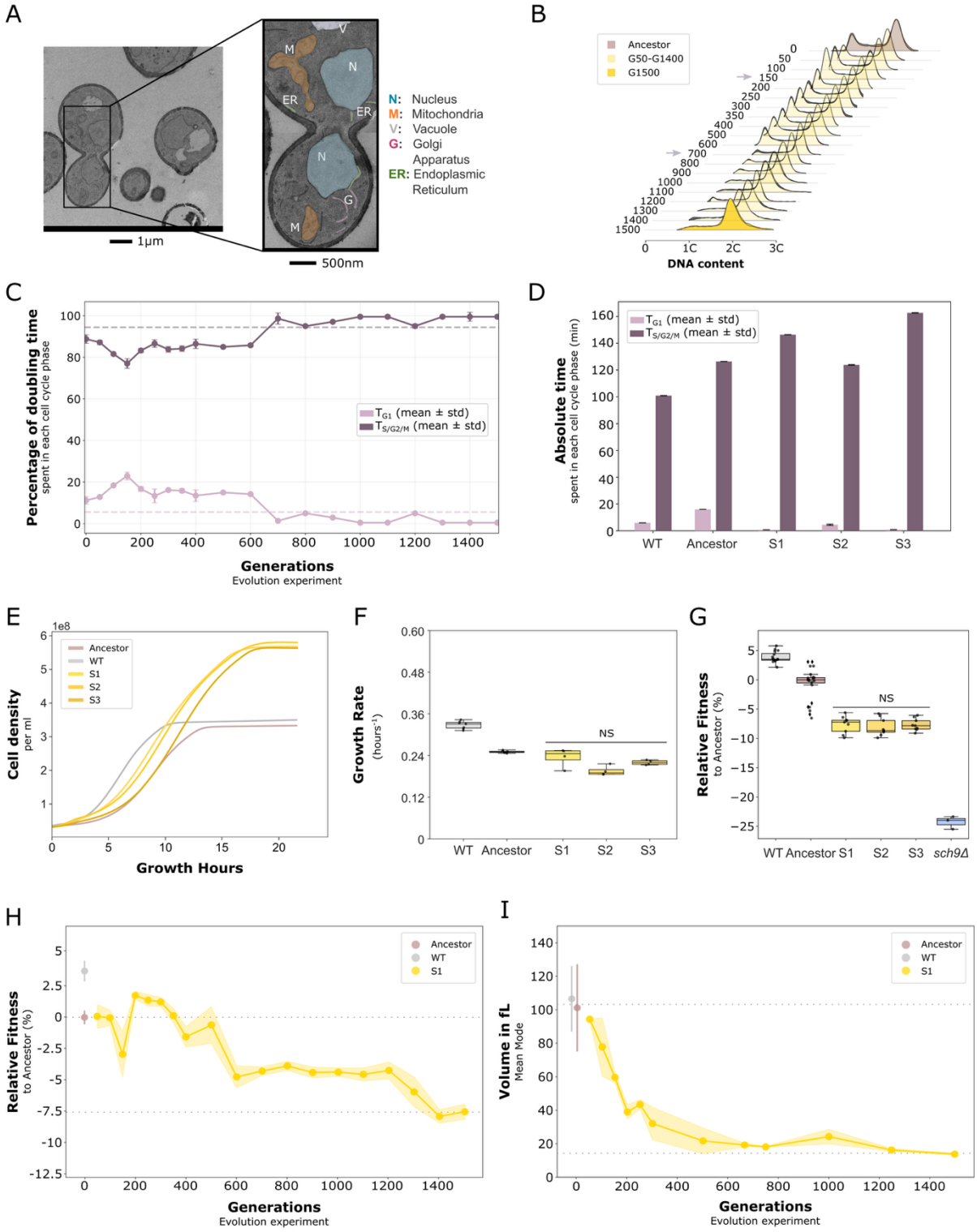

Figure 2. Physiology of cell miniaturization. (A) Transmission electron micrograph of evolved *S. cerevisiae* cells during exponential growth in YPD. Scale bar, 1 µm. (B) DNA-content profiles of ancestral and representative evolved (S1) populations during exponential growth across 1,500 generations, measured by flow cytometry. Lines show means; shaded areas, SD (n = 3). G2 peak height was normalized to 1. Arrows indicate time points of cell-cycle profile changes (see main text). (C) Percentage of doubling time spent in G1 and S/G2/M phases for the S1 population at generation 1,500. Bars show mean ± SD (n = 3). (D) Absolute time spent in each cell cycle phase, calculated as the fraction of the doubling time allocated to each phase. (E) Growth

curves of selected strains measured as cell density (cells/mL). (F) Maximum growth rates of reference and evolved strains (generation 1,500) in YPD. Box plots show medians, interquartile ranges, whiskers (1.5× IQR), and outliers. Statistical significance assessed by the Mann–Whitney–Wilcoxon test; p-values indicated. Differences among evolved lines (S1–S3) were not significant (adjusted p = 0.082–0.143), whereas growth rates differed significantly between wild type and evolved populations (p = 0.006). The ancestor did not differ from S1 (p = 0.65) but differed from S2 and S3 (p = 0.006; n = 4 each). Full pairwise statistics in RawData-Figures Table Fig2F. (G) Relative fitness of wild-type, ancestral, and evolved populations (S1–S3) at generation 1,500. Relative fitness is the ratio of reproductive success of a strain to a reference strain under identical conditions. Fitness of evolved and *sch9Δ* strains differed significantly from the ancestor and wild type (adjusted p < 0.01), with no significant differences among evolved lines. Box plots as in (F). Full pairwise statistics in RawData-Figures Table Fig2G. (H and I) Fitness and cell-size trajectories across 1,500 generations for the S1 population. Lines show mean values; shaded areas, SD.

New evolved size homeostasis is stable and robust

How stable is the evolved miniaturized size? Measurements performed right after the last sorting round may reflect a transient physiological state, rather than an evolutionarily stable phenotype. To address this possibility, clones were isolated from two independent populations (S1Cl2 and S2Cl4) and passaged for 150 generations in the absence of any size selection. Interestingly, S-clones stably maintained their size across the experiment, resulting in a smaller final fold change than the one observed in control WT lines (Figure 3A). In contrast, *sch9*Δ lines, consistently reverted to WT sizes between 50 and 100 generations despite starting with a larger volume than S-clones (Figure 3A). An important question is whether miniaturized cells actively regulate their size, or whether they merely preserve the volumes attained at the end of the experiment. To address this, we transiently arrested cells at the G1/S transition using the pheromone α-factor, which permits growth while blocking division (54) (Figure S3A and S3B). While the arrest was not fully efficient in S-clones, it nevertheless led to a ~1.8-fold increase in cell volume in both WT and evolved cells. The increased volume, however, was progressively reversed upon release into fresh medium, indicating that cells actively return to their characteristic size (Figure S3A, S3C).

The ability of miniaturized cells to maintain their size across many generations and under transient perturbations reflects efficient size homeostasis, which is expected to manifest as a

narrow distribution of cell sizes around the population mean. To test this prediction, we compared the size distributions of WT, ancestral strains, S-clones, and *sch9*Δ controls. Cell size distributions are described by a universal statistical structure (55), by which the distribution of rescaled cell sizes $V = v/\langle v \rangle$ is invariant across strains and species. Here, $\langle v \rangle$ denotes the mean size of a strain. This invariance leads to a "collapse" of rescaled cell size distributions onto a single curve (Figure 3B and 3C) and implies that the coefficient of variation (CV) of the original (non-rescaled) distributions is constant. Such rescaling enables meaningful comparison of size homeostasis across strains with markedly different sizes. *sch9*Δ controls showed a poor collapse of the rescaled distributions compared to WT (Figure 3C), accompanied by an increased CV ($p < 0.001$, Figure 3D), consistent with greater variability than expected for their mean size. By contrast, S-clones exhibited collapse and CV values close to WT (SI Appendix), leading to overlapping rescaled distributions with WT and ancestral strains (Figures 3B–D).

Together, these results demonstrate that miniaturized cells have evolved a new cell size homeostasis that is evolutionarily stable, robust to transient perturbations, and capable of maintaining population-level size control as tightly as WT.

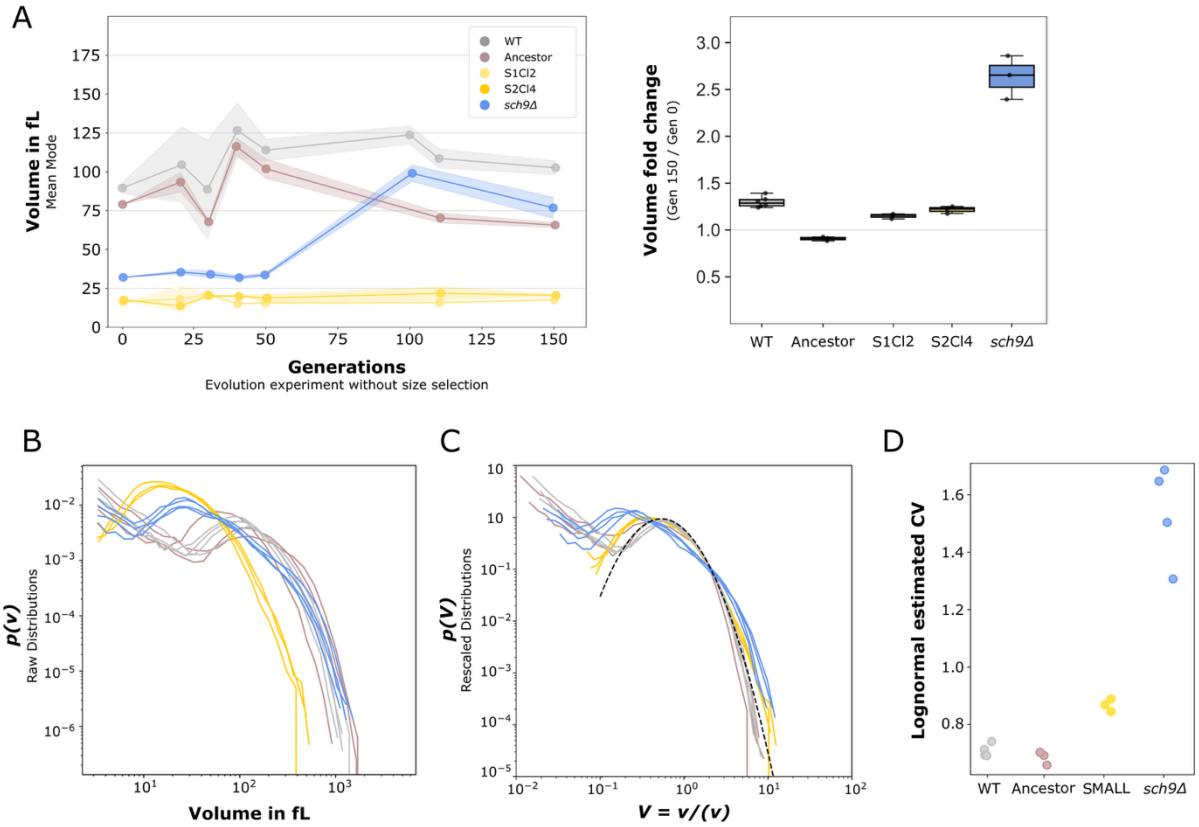

Figure 3. Evolution of cell size homeostasis. (A) Stability of cell size during experimental evolution. Left: cell-size measurements of WT, ancestor, *sch9Δ*, and evolved clones at 1,500 generations from populations evolved without size selection. No significant differences were detected between S1Cl2 and S2Cl4 replicates (Mann–Whitney U test, $p > 0.1$), indicating stable size maintenance. Right: fold change in cell size relative to time 0. (B) Distributions of cell volumes for the analyzed strains before rescaling. Leftmost peaks correspond to debris. (C) Collapse of rescaled cell-volume distributions around their mean, estimated using truncated log-normal fits applied to data above the mode to exclude debris. The dashed black curve shows the best log-normal fit to the rescaled, debris-corrected WT distribution (see Materials and Methods). (D) Coefficient of variation of the collapsed volume distributions, quantifying size variability after rescaling and revealing differences in size homeostasis among genotypes.

Genetic landscape of cellular miniaturization

We sought to determine the genetic basis of the evolved phenotype. Evolved cells retained their characteristic size when co-cultured with wild-type strains, indicating that miniaturization was not driven by secreted or diffusible factors (Figure S4A). The phenotype's persistence over 150 generations in the absence of selection (Figure 3A) strongly suggested a genetic basis. Supporting this idea, crosses between evolved clones and WT produced

239 diploids of intermediate size between haploid and diploid WT, consistent with the presence
240 of both recessive and dominant mutations. Furthermore, crosses of evolved clones with
241 derivatives whose mating type had been switched yielded diploids that maintained a 6-fold
242 volume reduction relative to WT diploids (Figure S4B), suggesting that the reduction of cell size
243 is independent of ploidy state.

244 To identify causative mutations, we performed whole-genome, whole-population sequencing
245 across multiple evolutionary timepoints. As expected from the mutator allele present in the
246 ancestral population, we detected 869 unique mutations that arose during evolution in coding
247 and regulatory regions across the three populations that were not present in the ancestor
248 (Figure 4A, Table S2). By the end of the experiment, an average of 267 single-nucleotide
249 polymorphisms (SNPs) and small insertions/deletions (indels) persisted per population (285
250 in S1, 301 in S2 and 216 in S3). No aneuploidies, segmental amplifications, or large-scale
251 changes in DNA copy number were observed, thus confirming the presence of a full haploid
252 genome (Figure S4D). The evolved populations exhibited distinct clonal compositions (Figure
253 S4C–D). However, several alleles were shared across populations, indicating that cross-
254 contamination likely occurred during the FACS selection steps. Consequently, the evolved
255 lines were treated as a single, large evolving population for subsequent analyses (Figure 4A).

256 To identify putative adaptive mutations associated with the evolved cell size, we employed
257 four non exhaustive, but complementary approaches: (i) tracking lineages that rose to fixation
258 in any of the three sub-populations, identifying cohorts of mutations under positive selection
259 (Table S2); (ii) searching for genes previously implicated in cell size regulation (Table S3); (iii)
260 using statistical inference to identify genes mutated more frequently than expected given their
261 size and the observed mutation rates (parallel evolution; Table S4); and (iv) performing two
262 consecutive rounds of backcrossing and selection for small cell size to pinpoint mutations
263 segregating with the phenotype (bulk segregant analysis; Table S5; see Materials and Methods

for details). A summary of the genes identified by these methods, as well as their reported interactions, is portrayed in Figure 4B-C (Table S6). Despite several genetic and physical interactions among the identified genes, no gene ontology term was found to be statistically enriched.

Our analysis indicates that the miniaturized phenotype is heritable and genetically encoded, but the underlying adaptive landscape is complex. The large number of candidate mutations likely includes false positives arising from hitchhiking or linkage, as well as variants under indirect selection. Some of these may reflect selection on traits influencing the flow-cytometry size proxy (FSC-A) rather than cell size itself, or compensatory adaptations to physiological changes associated with miniaturization (56).

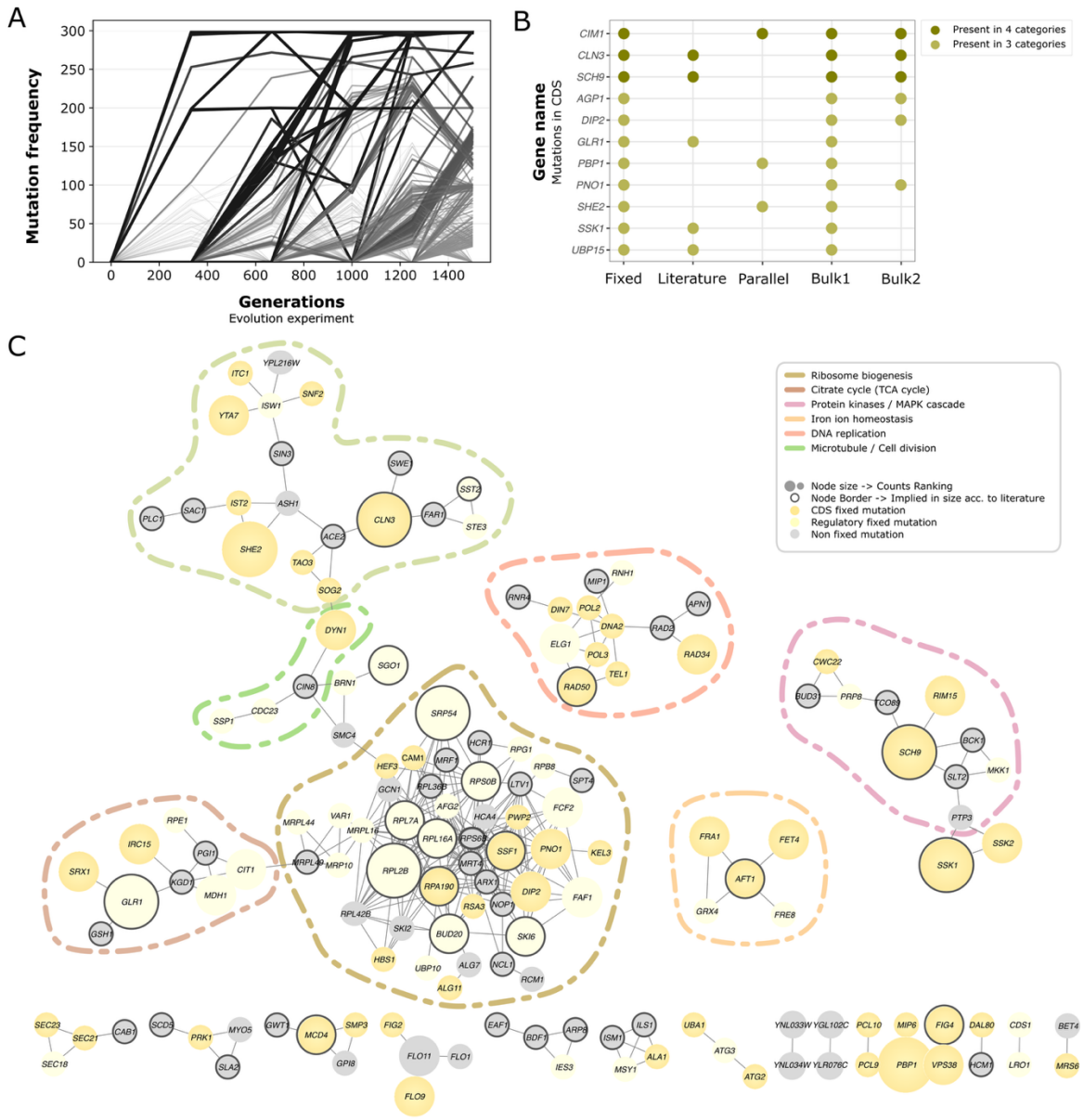

274

275 **Figure 4. Genomic landscape of the evolved phenotype.** (A) Allele-frequency trajectories of mutations detected in the
276 combined population (S1–S3). A 300% frequency indicates fixation in all three populations. Line thickness reflects the final
277 frequency of the mutation at generation 1,500. (B) List of putative adaptive gene mutations ranked by the number of satisfied
278 criteria outlined in the main text and affected by non-synonymous mutations located within coding sequences (CDS). Only
279 genes appearing in at least three categories are included (full list in Table S6). (C) Interaction network of mutations detected
280 in S1–S3 evolved populations curated in Cytoscape (52). Grey lines indicate known genetic and physical interactions
281 (STRING database (53)). Node diameter reflects the number of satisfied criteria we used to detect putative adaptive
282 mutations. Only genes appearing in at least two categories are included. Nodes are color-coded: dark yellow for non-
283 synonymous mutations within CDS fixed at generation 1,500, light yellow for mutations in the regulatory regions fixed at
284 generation 1,500, and grey for non-fixed mutations. Bold outlines mark genes linked to cell size changes in the literature
285 (either decrease or increase).

286 **Combined mutations in the G1 cyclin and Greatwall signalling cascades cause large**
287 **deviations in cell size**

288 We set out to identify the mutations primarily responsible for the change in cell size among
289 those identified as putatively adaptive. *CIM1*, *CLN3*, and *SCH9* ranked highest in our analysis
290 and were therefore selected for further investigation. *CIM1* encodes for a mitochondrial HMG-
291 box protein that limits mitochondrial DNA copy numbers (57), and independently
292 accumulated up to 6 mutations in the protein over the course of the experiment, including
293 three frameshifts resulting in premature stop codons (Figure S5A). Cln3, a G1 cyclin that
294 partners with Cdk1 to drive the G1/S transition by activating phase-specific gene expression,
295 has been shown to reduce cell size when truncated at its C-terminus (e.g. *cln3-1*), due to
296 increased protein stability (58, 59). Our evolved strains carried a similar truncation, *cln3-*
297 *S410**, just downstream of the *cln3-1* allele (Figure 5A). Sch9 is a key effector of the TORC1
298 pathway, which integrates nutrient sensing with anabolic and catabolic processes. We
299 identified a mutation (*sch9*-L343S) within the conserved C2 domain (residues 184–402), a
300 calcium-dependent membrane-targeting module that may also inhibit the kinase domain
301 (residues 403–738; Figure 5A, (60)). The influence of Sch9 on cell size has traditionally been
302 attributed to its role in ribosome biogenesis (47). However, recent work suggests an additional
303 function in regulating cell size through the Greatwall kinase Rim15, albeit under conditions of
304 low CDK activity (61). The Greatwall kinase cascade is highly conserved among eukaryotes
305 and regulates the cell cycle in humans and *Xenopus* via endosulfines-mediated inhibition of
306 the phosphatase PP2A (62, 63). Notably, whereas in *S. pombe* this pathway links nutrient
307 sensing to cell size (64), in *S. cerevisiae* it is thought to function mainly in the regulation of
308 quiescence (65). Interestingly, we also identified a fixed mutation in *RIM15* (*rim15-A132T*) and
309 another in *CDC55* (*cdc55-L159P*), which encodes a regulatory subunit of PP2A (66), though at
310 a lower frequency.

311 We tested the causality of the *cim1*, *cln3*, *sch9* and *rim15* mutant alleles by reconstructing
312 them in a WT background. We mimicked frameshift mutations in *CIM1* with a gene deletion,
313 which did not cause any change in cell size (Figure S5A), perhaps reflective of an adaptive role
314 in other cellular features or fitness. Mutations in *CLN3*, *SCH9*, and *RIM15* individually caused
315 a marginal but significant decrease in volumes compared to WT (Figure 5C-D). Combinations
316 of the three mutations lead to additive and synergistic effects, with the triple mutant
317 producing a three-fold reduction in volume (28.5 fL, Figure 5C). Although *sch9-L343S cln3-*
318 *S410** double mutant already manifested a small cell size, the additional *rim15-A132T* allele
319 marginally decreased the volume (p= 3.2587e-03, Figure 5C and S5B). To further test the
320 involvement of Rim15 in the final evolved size, we engineered a tunable promoter (*prCUP1*)
321 driving the *RIM15* and *rim15-A132T* alleles. Copper titration confirmed Rim15 dosage
322 sensitivity: basal expression reduced size, and overexpression caused further shrinkage in
323 both WT and *cln3-S410** backgrounds (Figure S5C). Notably, overexpressing *rim15-A132T* in
324 the *sch9-L343S cln3-S410** background decreased size even further, matching that of the final
325 evolved clones (16 fL ± 0.1 (mean ± SD), Figure 5C and S5C). These results suggest that, in
326 addition to a gain of function of the G1 cyclin Cln3, a gain of function of the Greatwall signaling
327 cascade may be responsible for the miniaturized volume. Consistent with this, deleting *RIM15*
328 in evolved clones restored larger volumes (Figure S5D). Importantly, despite their small size,
329 all strains reconstructed with evolved alleles retained near-WT fitness (Figure 5C). The
330 engineered *prCUP1-rim15-A132T* in the *sch9-L343S cln3-S410** background resulted in lower
331 fitness than the evolved clones but higher than *sch9Δ*. However, these fitness levels likely
332 reflect the toxic effects of deregulated *Rim15* expression throughout the cell cycle rather than
333 reduced cell size, as fitness remained constant while size decreased at higher copper
334 concentrations (Figure 5C).

335 Finally, following the hypothesis that the combined effect of the reconstructed mutations
336 results in a gain of function in the G1 cyclin and Greatwall signaling cascades, we asked

337 whether removing Cln3 and Rim15 would enlarge cell size. Indeed, simultaneous deletion of

338 *CLN3* and *RIM15* produced a synergistic ~2.3-fold volume increase (Figure 5E). Altogether,

339 combining alleles that modulate G1 cyclin activity and Greatwall signalling generated a

340 fourteen-fold size range, comparable to 82.86% of the variation in sizes observed across the

341 entire *Saccharomycotina* subphylum (Figure 5E).

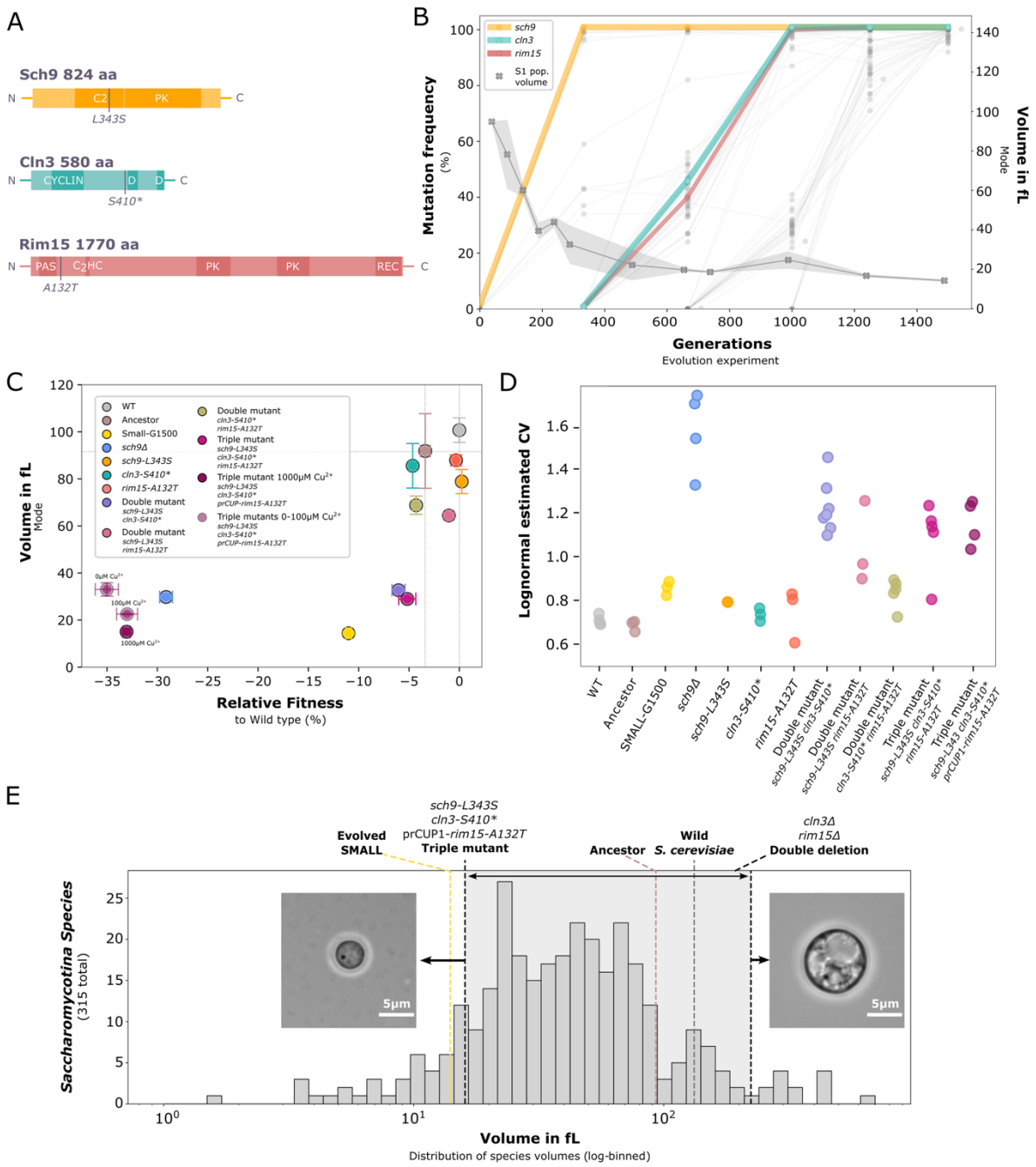

342

343 **Figure 5. Genetic basis of cell size phenotype.** (A) Schematic of cell size–regulating genes. Protein domains are indicated,
344 and mutations identified during evolution are marked: PK, kinase catalytic domain; D, consensus disorder prediction; PAS, N-
345 terminal PAS; C2HC, CCHC-type zinc-finger domains; REC, C-terminal receiver domain. (B) Allele-frequency trajectories of size-
346 associated mutations. Only variants reaching ≥80% frequency by generation 1,500 are shown; causative mutations are
347 highlighted. The right axis shows the S1 population volume (× symbols) over time. (C) Relationship between relative fitness and
348 modal cell volume. Each point represents a strain (WT, ancestor, evolved populations, or engineered mutants). Fitness (x-axis)
349 and cell volume (y-axis); error bars indicate SD. (D) Coefficient of variation of rescaled volume distributions, quantifying size
350 variability and differences in size homeostasis among genotypes. (E) Distribution of cell volumes across the *Saccharomycotina*
351 subphylum (derived from (50)). Highlighted are the triple mutant (*sch9-L343S cln3-S410* prCUP1-rim15-A132T*) under a copper-
352 inducible promoter and the *CLN3* and *RIM15* double deletions, showing shifts in size relative to natural variation.

353 **DISCUSSION**

354 How can evolution produce large shifts in cell size without incurring in the detrimental effects
355 associated with even small deviations from the norm? In development, abrupt changes often
356 arise through ploidy increase or reduction, and cell volume scales linearly with DNA content
357 across taxa (67). Ploidy increases are important in plant evolution and likely account for part
358 of the variation in cell size among related species (68). Yet, genome duplications alone cannot
359 explain the wide diversity of cell sizes, as they also create barriers to sexual reproduction and
360 would leave more pervasive genomic signatures if they were the main driver. Cells must
361 therefore be able to modify size independently of DNA content, at least initially, especially
362 under gradual selection for divergent sizes.

363 Decades of studies on eukaryotic cell cycle regulation have identified the main principles
364 allowing cells to regulate their size, as well as many molecular players involved (reviewed in
365 (10, 69). Mutations in many such players have been demonstrated to produce altered sizes
366 (34, 35, 70). It is therefore intuitive to imagine that evolution could modulate cell size by fine-
367 tuning these molecular players. Yet most such mutations reduce fitness, and it remains
368 unclear which, if any, combinations of the dozens of known regulators could provide viable
369 evolutionary paths to new cell sizes.

370 We addressed this question experimentally by imposing selection on *S. cerevisiae* cell size
371 and fitness. Over 1,500 generations, cells shrank six-fold in volume without changes in ploidy
372 and with minimal fitness costs. We show that miniaturized cells maintain an efficient and
373 evolutionarily stable cell size homeostasis, despite a significantly altered cell cycle
374 progression characterized by the near absence of a G1 phase. Whole genome sequencing
375 revealed a complex genomic landscape, due to the mutator allele employed, and likely linked
376 to the many direct and indirect changes cells experienced during the miniaturization.
377 Nevertheless, re-engineering putative adaptive alleles showed that simultaneous
378 perturbations of the G1 cyclin *CLN3* and the Greatwall kinase *RIM15* pathways recapitulate
379 the miniaturized phenotype, whereas loss-of-function in the same genes drives cell
380 enlargement. Together, manipulations in these signaling cascades produced a fourteen-fold
381 size range within a constant genome, capturing up to 82.86% (261 / 315) of the natural
382 variation in size seen across the *Saccharomycotina* over 400 million years of evolution.

383 Three questions arise. First, how can our evolved cells reach sizes smaller than those
384 achieved previously through gene deletions? We propose that evolution selected alleles with
385 modest individual effects, but that act synergistically on cell size by working on multiple
386 mechanisms simultaneously. We speculate the following model to account for the phenotype
387 observed (Figure 6): Truncations in *CLN3* stabilize the protein, increasing *CDK1–Cln3* activity
388 and phosphorylation of the transcriptional inhibitor Whi5 (71). In parallel, gain-of-function
389 mutations in the Greatwall kinase Rim15 enhance Igo1/2-mediated inhibition of the
390 phosphatase PP2A–Cdc55, further driving Whi5 phosphorylation and nuclear exclusion (61).
391 But why would this lead to a volume smaller than *whi5Δ* (Figure S5E), where the inhibitor is
392 absent? First, CDK1-Cln3 levels could simultaneously hyper-phosphorylate the
393 transcriptional regulator Stb1 (19, 72, 73) and accelerate the degradation of the CDK1
394 inhibitor Sic1 (74–76), eliminating the G1 phase. Furthermore, *RIM15* activity in mitosis has

395 been reported to destabilize the CDK1 inhibitor and size/morphogenesis checkpoint Swe1
396 (77), offering an additional route to reduced volume.

397 The second question regards what allows these miniaturized cells to retain high fitness.
398 Eukaryotic cells physiologically shrink upon nutrient scarcity (12), where cells may find it
399 advantageous to increase population-wide survival by dividing at a smaller volume while making
400 a parsimonious use of the resources left by reducing ribosome biogenesis. We propose that the
401 deletion of *SCH9* hard-wires this response, resulting in severe fitness defects due to strongly
402 decreased protein production. We speculate that the allele we obtained is a separation-of-
403 function allele, which interferes with Sch9's ability to inhibit the Greatwall kinase, but allows the
404 signaling that promotes ribosome biogenesis.

405 Finally, our miniaturized cells spend virtually no time in G1, yet they maintain robust size
406 homeostasis at the population level. The G1 duration is thought to buffer stochastic differences
407 in birth size (14, 17). Does the G1/S transition still perform this function on such short timescales,
408 or has size control shifted to a cryptic checkpoint in another phase, such as G2/M, as observed
409 in *S. pombe?*

410 In summary, our work shows how cell cycle regulation alone can achieve large deviations in cell
411 size while maintaining homeostasis. It also identifies a simple yet powerful route for evolution to
412 simultaneously modulate the G1 cyclin and Greatwall kinase pathways synergistically to control
413 the time spent in G1/G2, and thus cells' ability to grow in interphase. Finally, by coordinating
414 multiple points of size control while preserving biosynthetic capacity, cells can achieve large
415 deviations in volume without altering ploidy. Future studies should test the generality of the
416 principles we identified and determine how broadly it underpins size diversity across the tree of
417 life.

418 Overall, our work illustrates how long-term evolution, quantitative physiology, and molecular
419 genetics, together, can inform the mechanisms underlying the evolution of cellular traits (78).

420 The generation of an unprecedented range of cell sizes within one species, with proliferating
421 cells and stable ploidy, provides a useful framework for future work on subcellular scaling and
422 the limits of cell size.

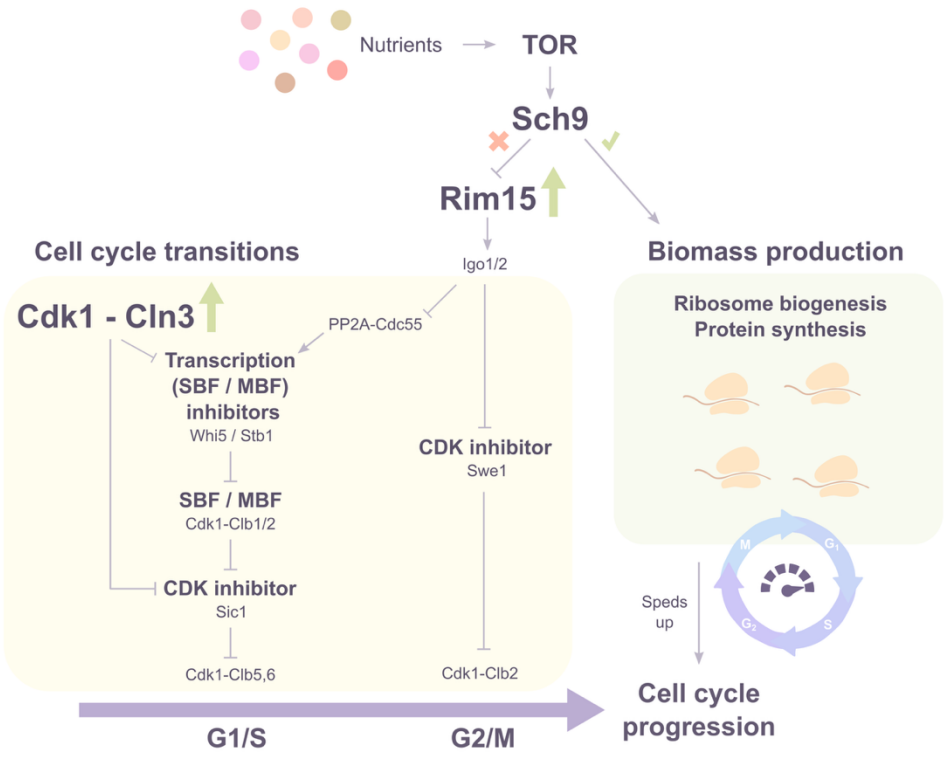

423

424 **Figure 6. Speculative model of the effect of the mutations identified on cell cycle regulation.** In wild-type (WT) cells
425 growing under nutrient-rich conditions, TOR is active, promoting ribosome biogenesis and biomass accumulation (right, green
426 rectangle) while delaying cell cycle transitions (left, orange rectangle). This results in fast-growing, large cells. Under nutrient
427 limitation or in TOR-related mutants, Sch9 repression of Rim15 is relieved, leading to earlier cell cycle transitions. However,
428 the accompanying reduction in biomass production limits growth and fitness. We propose that the combined effect of the
429 identified mutations accelerates cell cycle transitions while maintaining ribosome biogenesis and biomass production. As a
430 result, cells grow rapidly but, by spending less time in interphase, remain smaller than their WT counterparts.

431

432 **MATERIAL AND METHODS**

433 All strains used in this study were W303 derivatives. Yeast cultures were propagated using
434 standard techniques (79). Unless otherwise stated, experiments were performed in standard rich
435 medium (YPD). Experimental evolution followed the procedure described in (80), with the

436 addition of the size-selection step by sorting detailed in the SI Appendix. Growth-curve
437 measurements and fitness assays were performed as described in (81). Samples for cell-cycle
438 analyses were processed as (81) and analyzed as in (82). Whole-genome sequencing and
439 analysis followed procedures described in (83). A full description of all methods is provided in
440 the SI Appendix, Methods.

441 **Data Availability**

442 The genomic datasets used within this publication were deposited at European Nucleotide
443 Archive (PRJEB101156). Scripts used for data analysis are available at the GitHub repository
444 (https://github.com/FumaLab/Garona2025). The raw data corresponding to each figure are
445 provided in the Raw Data–Figures Table. Expanded view data, supplementary information, and
446 appendices are available for this paper.

447 **Authors contribution**

448 M.F. conceived the project. A.Ga. and M.F. designed the research, performed the experiments,
449 and analyzed the data. A.Gi. contributed data analysis for Figure 3B–D. M.V.L. contributed
450 experimental work for Figure 5C, E. A.Ga. and M.F. wrote the original manuscript draft. All authors
451 edited and commented on the final version of the manuscript.

452 **Acknowledgments**

453 We thank Mina Abrantes, Joana Boas, Filipa Cantanhede, Olga Carreira, and João Martins for
454 their assistance in the experimental work; all the members of the Genome Maintenance and
455 Evolution lab for daily support helpful discussions; Gabriel Neurohr, Andrew W. Murray, Paula
456 Gonçalves, Partha Pratim Chakraborty and Mariana Natalino for critical reading of the
457 manuscript. The Flow Cytometry, Electron Microscopy, Bioimaging, and Genomics Facility of the
458 Gulbenkian Institute for Molecular Medicine for their technical support. We also thank Beatriz

Tomaz, Erin Tranfield and Muriel Christel Mari for their help in the establishment of the electron microscopy sample preparation. The authors acknowledge support from the Gulbenkian Foundation and the Gulbenkian Institute for Molecular Medicine (A.Ga., M.V.L and M.F), the Human Frontier Science Program (HFSP) -RGEC28/2023 (M.F and A.Gi), European Molecular Biology Organization (EMBO) - IG 5349-2023 (M.F), Fundação para a Ciência e a Tecnologia (FCT) - 2023.09068.CEECIND (M.F) and the National Institute of General Medical Sciences (NIGMS) of the National Institutes of Health (NIH), United States of America, 1R35GM147493 (A.Gi).

BIBLIOGRAPHY

1. M. B. Ginzberg, R. Kafri, M. Kirschner, Cell biology. On being the right (cell) size. *Science* **348**, 1245075 (2015).

2. C. Cadart, R. Heald, Scaling of biosynthesis and metabolism with cell size. *Mol. Biol. Cell* **33** (2022).

3. T. P. Miettinen, M. J. Caldez, P. Kaldis, M. Björklund, Cell size control - a mechanism for maintaining fitness and function. *Bioessays* **39**, 1700058 (2017).

4. T. L. Orr-Weaver, When bigger is better: the role of polyploidy in organogenesis. *Trends Genet.* **31**, 307–315 (2015).

5. M. G. Gabridge, Current status of the mycoplasmas: The smallest living cells. *Lab. Med.* **9**, 36–40 (1978).

6. J.-M. Volland, *et al.*, A centimeter-long bacterium with DNA contained in metabolically active, membrane-bound organelles. *Science* **376**, 1453–1458 (2022).

7. M.-J. Chrétiennot-Dinet, *et al.*, A new marine picoeucaryote: Ostreococcus tauri gen. et sp. nov. (Chlorophyta, Prasinophyceae). *Phycologia* **34**, 285–292 (1995).

8. C. Di Meo, G. Stanco, M. I. Cutrignelli, S. Castaldo, A. Nizza, Physical and chemical quality of ostrich eggs during the laying season. *Br. Poult. Sci.* **44**, 386–390 (2003).

9. R. Milo, R. Philips, Cell Biology by the Numbers. Available at: https://book.bionumbers.org/ [Accessed 23 October 2025].

10. A. A. Amodeo, J. M. Skotheim, Cell-Size Control. *Cold Spring Harb. Perspect. Biol.* **8**, a019083 (2016).

11. N. Rhind, Cell-size control. *Curr. Biol.* **31**, R1414–R1420 (2021).

12. G. C. Johnston, J. R. Pringle, L. H. Hartwell, Coordination of growth with cell division in the yeast Saccharomyces cerevisiae. *Exp. Cell Res.* **105**, 79–98 (1977).

13. X. Liu, J. Yan, M. W. Kirschner, Cell size homeostasis is tightly controlled throughout the cell cycle. *PLoS Biol.* **22**, e3002453 (2024).

14. L. H. Hartwell, M. W. Unger, Unequal division in Saccharomyces cerevisiae and its implications for the control of cell division. *J. Cell Biol.* **75**, 422–435 (1977).

15. D. Killander, A. Zetterberg, Quantitative cytochemical studies on interphase growth. I. Determination of DNA, RNA and mass content of age determined mouse fibroblasts in vitro and of intercellular variation in generation time. *Exp. Cell Res.* **38**, 272–284 (1965).

16. P. Nurse, Genetic control of cell size at cell division in yeast. *Nature* **256**, 547–551 (1975).

17. I. Soifer, L. Robert, A. Amir, Single-Cell Analysis of Growth in Budding Yeast and Bacteria Reveals a Common Size Regulation Strategy. *Curr. Biol.* **26**, 356–361 (2016).

18. E. Vergés, N. Colomina, E. Garí, C. Gallego, M. Aldea, Cyclin Cln3 is retained at the ER and released by the J chaperone Ydj1 in late G1 to trigger cell cycle entry. *Mol. Cell* **26**, 649–662 (2007).

19. H. Wang, L. B. Carey, Y. Cai, H. Wijnen, B. Futcher, Recruitment of Cln3 cyclin to promoters controls cell cycle entry via histone deacetylase and other targets. *PLoS Biol.* **7**, e1000189 (2009).

20. K. M. Schmoller, J. J. Turner, M. Kõivomägi, J. M. Skotheim, Dilution of the cell cycle inhibitor Whi5 controls budding-yeast cell size. *Nature* **526**, 268–272 (2015).

21. X. Liu, *et al.*, Reliable cell cycle commitment in budding yeast is ensured by signal integration. *Elife* **4** (2015).

22. S. Dorsey, *et al.*, G1/S transcription factor copy number is a growth-dependent determinant of cell cycle commitment in yeast. *Cell Syst.* **6**, 539-554.e11 (2018).

23. F. S. Heldt, R. Lunstone, J. J. Tyson, B. Novák, Dilution and titration of cell-cycle regulators may control cell size in budding yeast. *PLoS Comput. Biol.* **14**, e1006548 (2018).

24. A. Litsios, *et al.*, Differential scaling between G1 protein production and cell size dynamics promotes commitment to the cell division cycle in budding yeast. *Nat. Cell Biol.* **21**, 1382–1392 (2019).

25. Y. Chen, G. Zhao, J. Zahumensky, S. Honey, B. Futcher, Differential Scaling of Gene Expression with Cell Size May Explain Size Control in Budding Yeast. *Mol. Cell* **78**, 359-370.e6 (2020).

26. Z. N. Demidenko, M. V. Blagosklonny, Growth stimulation leads to cellular senescence when the cell cycle is blocked. *Cell Cycle* **7**, 3355–3361 (2008).

27. G. E. Neurohr, *et al.*, Excessive Cell Growth Causes Cytoplasm Dilution And Contributes to Senescence. *Cell* **176**, 1083-1097.e18 (2019).

28. J. Lengefeld, *et al.*, Cell size is a determinant of stem cell potential during aging. *Sci Adv* **7**, eabk0271 (2021).

29. M. C. Lanz, *et al.*, Increasing cell size remodels the proteome and promotes senescence. *Mol. Cell* **82**, 3255-3269.e8 (2022).

30. S. Manohar, *et al.*, Genome homeostasis defects drive enlarged cells into senescence. *Mol. Cell* **83**, 4032-4046.e6 (2023).

31. L. Crozier, *et al.*, CDK4/6 inhibitor-mediated cell overgrowth triggers osmotic and replication stress to promote senescence. *Mol. Cell* **83**, 4062-4077.e5 (2023).

32. R. Foy, *et al.*, Oncogenic signals prime cancer cells for toxic cell overgrowth during a G1 cell cycle arrest. *Mol. Cell* **83**, 4047-4061.e6 (2023).

33. S. Manohar, G. E. Neurohr, Too big not to fail: emerging evidence for size-induced senescence. *FEBS J.* **291**, 2291–2305 (2024).

34. P. Jorgensen, J. L. Nishikawa, B.-J. Breitkreutz, M. Tyers, Systematic Identification of Pathways That Couple Cell Growth and Division in Yeast. *Science* **297**, 395–400 (2002).

35. J. Zhang, *et al.*, Genomic Scale Mutant Hunt Identifies Cell Size Homeostasis Genes in S. cerevisiae. *Curr. Biol.* **12**, 1992–2001 (2002).

36. M. Ohanna, *et al.*, Atrophy of S6K1(-/-) skeletal muscle cells reveals distinct mTOR effectors for cell cycle and size control. *Nat. Cell Biol.* **7**, 286–294 (2005).

37. S. M. I. Goorden, *et al.*, Rheb is essential for murine development. *Mol. Cell. Biol.* **31**, 1672–1678 (2011).

38. C. D. Bell, E. Waizbard, Variability of cell size in primary and metastatic human breast carcinoma. *Invasion Metastasis* **6**, 11–20 (1986).

39. B. M. Iritani, R. N. Eisenman, c-Myc enhances protein synthesis and cell size during B lymphocyte development. *Proc. Natl. Acad. Sci. U. S. A.* **96**, 13180–13185 (1999).

40. I. Jones, *et al.*, Characterization of proteome-size scaling by integrative omics reveals mechanisms of proliferation control in cancer. *Sci. Adv.* **9**, eadd0636 (2023).

41. Asadullah, *et al.*, Combined heterogeneity in cell size and deformability promotes cancer invasiveness. *J. Cell Sci.* **134**, jcs250225 (2021).

42. T. J. Kawecki, *et al.*, Experimental evolution. *Trends Ecol. Evol.* **27**, 547–560 (2012).

43. M. Natalino, M. Fumasoni, Experimental approaches to study evolutionary cell biology using yeasts. *Yeast* **40**, 123–133 (2023).

44. J. Helsen, G. Sherlock, G. Dey, Experimental evolution for cell biology. *Trends Cell Biol.* **33**, 903–912 (2023).

45. Practical Flow Cytometry Shapiro, 4th Edition.

46. Y. H. Jin, *et al.*, The multiple biological roles of the 3'-->5' exonuclease of Saccharomyces cerevisiae DNA polymerase delta require switching between the polymerase and exonuclease domains. *Mol. Cell. Biol.* **25**, 461–471 (2005).

47. P. Jorgensen, *et al.*, A dynamic transcriptional network communicates growth potential to ribosome synthesis and critical cell size. *Genes Dev.* **18**, 2491–2505 (2004).

48. P. Russell, P. Nurse, cdc25+ functions as an inducer in the mitotic control of fission yeast. *Cell* **45**, 145–153 (1986).

49. K. Lundgren, *et al.*, Mik1 and wee1 cooperate in the inhibitory tyrosine phosphorylation of cdc2. *Cell* **64**, 1111–1122 (1991).

50. C. M. Chavez, *et al.*, The cell morphological diversity of Saccharomycotina yeasts. *FEMS Yeast Res.* **24**, foad055 (2024).

51. M. Osumi, Visualization of yeast cells by electron microscopy. *J. Electron Microsc.* **61**, 343–365 (2012).

52. D. H. Williamson, A. W. Scopes, The behaviour of nucleic acids in synchronously dividing cultures of Saccharomyces cerevisiae. *Exp. Cell Res.* **20**, 338–349 (1960).

53. R. E. Lenski, M. R. Rose, S. C. Simpson, S. C. Tadler, Long-Term Experimental Evolution in Escherichia coli . I . Adaptation and Divergence During. *Am. Nat.* **138**, 1315–1341 (1991).

54. A. I. Goranov, *et al.*, The rate of cell growth is governed by cell cycle stage. *Genes Dev.* **23**, 1408–1422 (2009).

55. A. Giometto, F. Altermatt, F. Carrara, A. Maritan, A. Rinaldo, Scaling body size fluctuations. *Proceedings of the National Academy of Sciences* **110**, 4646–4650 (2013).

56. T. LaBar, Y. Y. Phoebe Hsieh, M. Fumasoni, A. W. Murray, Evolutionary Repair Experiments as a Window to the Molecular Diversity of Life. *Curr. Biol.* **30**, R565–R574 (2020).

57. S. Schrott, C. Osman, Two mitochondrial HMG-box proteins, Cim1 and Abf2, antagonistically regulate mtDNA copy number in Saccharomyces cerevisiae. *Nucleic Acids Res.* **51**, 11813–11835 (2023).

58. B. L. A. Carter, P. E. Sudbery, SMALL-SIZED MUTANTS OF SACCHAROMYCES CEREVISIAE. *Genetics* **96**, 561–566 (1980).

59. M. Tyers, G. Tokiwa, R. Nash, B. Futcher, The Cln3-Cdc28 kinase complex of S. cerevisiae is regulated by proteolysis and phosphorylation. *EMBO J.* **11**, 1773–1784 (1992).

60. M. Caligaris, *et al.*, Snf1/AMPK fine-tunes TORC1 signaling in response to glucose starvation. *Elife* **12** (2023).

61. N. Talarek, E. Gueydon, E. Schwob, Homeostatic control of START through negative feedback between Cln3-Cdk1 and Rim15/Greatwall kinase in budding yeast. *Elife* **6** (2017).

62. S. Mochida, S. L. Maslen, M. Skehel, T. Hunt, Greatwall phosphorylates an inhibitor of protein phosphatase 2A that is essential for mitosis. *Science* **330**, 1670–1673 (2010).

63. A. Gharbi-Ayachi, *et al.*, The substrate of Greatwall kinase, Arpp19, controls mitosis by inhibiting protein phosphatase 2A. *Science* **330**, 1673–1677 (2010).

603 64. N. Chica, *et al.*, Nutritional control of cell size by the greatwall-endosulfine-PP2A·B55
604 pathway. *Curr. Biol.* **26**, 319–330 (2016).

605 65. S. Bontron, *et al.*, Yeast endosulfines control entry into quiescence and chronological
606 life span by inhibiting protein phosphatase 2A. *Cell Rep.* **3**, 16–22 (2013).

607 66. A. M. Healy, *et al.*, CDC55, a Saccharomyces cerevisiae gene involved in cellular
608 morphogenesis: identification, characterization, and homology to the B subunit of
609 mammalian type 2A protein phosphatase. *Mol. Cell. Biol.* **11**, 5767–5780 (1991).

610 67. T. R. Gregory, Coincidence, coevolution, or causation? DNA content, cell size, and the
611 C-value enigma. *Biol. Rev. Camb. Philos. Soc.* **76**, 65–101 (2001).

612 68. J. S. P. Heslop-Harrison, T. Schwarzacher, Q. Liu, Polyploidy: its consequences and
613 enabling role in plant diversification and evolution. *Ann. Bot.* **131**, 1–10 (2023).

614 69. Y. Chadha, A. Khurana, K. M. Schmoller, Eukaryotic cell size regulation and its
615 implications for cellular function and dysfunction. *Physiol. Rev.* **104**, 1679–1717 (2024).

616 70. I. Soifer, N. Barkai, Systematic identification of cell size regulators in budding yeast.
617 *Mol. Syst. Biol.* **10**, 761 (2014).

618 71. R. A. M. de Bruin, W. H. McDonald, T. I. Kalashnikova, J. Yates 3rd, C. Wittenberg, Cln3
619 activates G1-specific transcription via phosphorylation of the SBF bound repressor
620 Whi5. *Cell* **117**, 887–898 (2004).

621 72. Y. Ho, M. Costanzo, L. Moore, R. Kobayashi, B. J. Andrews, Regulation of transcription at
622 the Saccharomyces cerevisiae start transition by Stb1, a Swi6-binding protein. *Mol.*
623 *Cell. Biol.* **19**, 5267–5278 (1999).

624 73. R. A. M. de Bruin, T. I. Kalashnikova, C. Wittenberg, Stb1 collaborates with other
625 regulators to modulate the G_1-specific transcriptional circuit. *Mol. Cell. Biol.* **28**, 6919–
626 6928 (2008).

627 74. R. Verma, *et al.*, Phosphorylation of Sic1p by G1 Cdk required for its degradation and
628 entry into S phase. *Science* **278**, 455–460 (1997).

629 75. M. Costanzo, *et al.*, CDK activity antagonizes Whi5, an inhibitor of G1/S transcription in
630 yeast. *Cell* **117**, 899–913 (2004).

631 76. F. R. Cross, L. Schroeder, J. M. Bean, Phosphorylation of the Sic1 inhibitor of B-type
632 cyclins in Saccharomyces cerevisiae is not essential but contributes to cell cycle
633 robustness. *Genetics* **176**, 1541–1555 (2007).

634 77. M. A. Juanes, *et al.*, Budding yeast greatwall and endosulfines control activity and
635 spatial regulation of PP2A(Cdc55) for timely mitotic progression. *PLoS Genet.* **9**,
636 e1003575 (2013).

637 78. M. Lynch, *et al.*, Evolutionary cell biology: two origins, one objective. *Proc. Natl. Acad.*
638 *Sci. U. S. A.* **111**, 16990–16994 (2014).

639 79. *Guide to yeast genetics and molecular biology* (Academic Press, 1990).

80. M. Fumasoni, A. W. Murray, The evolutionary plasticity of chromosome metabolism allows adaptation to constitutive DNA replication stress. *Elife* **9**, 1–28 (2020).

81. M. Natalino, M. Fumasoni, Compensatory evolution to DNA replication stress is robust to nutrient availability. *Mol. Syst. Biol.* (2025). https://doi.org/10.1038/s44320-025-00127-z.

82. A. Alsina, M. Fumasoni, P. Sartori, Model-based inference of cell cycle dynamics captures alterations of the DNA replication programme. *PLoS Comput. Biol.* **21**, e1013570 (2025).

83. M. Fumasoni, A. W. Murray, Ploidy and recombination proficiency shape the evolutionary adaptation to constitutive DNA replication stress. *PLoS Genet.* **17**, e1009875 (2021).